A nanoporous surface is essential for glomerular podocyte differentiation in three-dimensional culture

Cristina Zennaro[1], Maria Pia Rastaldi[2], Gerald James Bakeine[3], Riccarda Delfino[1], Federica Tonon[1], Rossella Farra[4], Gabriele Grassi[1,5], Mary Artero [6], Massimo Tormen[7], Michele Carraro[1].

[1] Department of Medical, Surgical and Health Sciences, University of Trieste, Trieste, Strada di Fiume 447, I-34149 Trieste, Italy.

[2] Fondazione IRCCS Ca' Granda Ospedale Maggiore Policlinico, Via Francesco Sforza 35, I-20122 Milano, Italy.

[3] Department of Radiology, San Martino University Hospital, University of Genoa, Largo Rosanna Benzi, 10, I-16132 Genova, Italy

[4] Department of Engineering and Architecture, University of Trieste, Via Alfonso Valerio, 6/A, I-34127 Trieste, Italy

[5] Department of Life Sciences, Cattinara University Hospital, Trieste University, Strada di Fiume 447, I-34149 Trieste, Italy

[6] Azienda Ospedaliero-Universitaria" Ospedali Riuniti di Trieste", Strada di Fiume 447, I-34149 Trieste, Italy

[7] IOM-CNR Area Science Park, Basovizza, S.S. 14,Km. 163.5, 34149 Trieste, Italy

Corresponding Author:

Dr Cristina Zennaro
Department of Medical, Surgical and Health Sciences
University of Trieste
Cattinara Hospital
Strada di Fiume 447
I-34149 Trieste
Telephone Number: +39 040 3996229
e-mail: czennaro@units.it

Abstract

Although it is well-recognized that cell-matrix interactions are based on both molecular and geometrical characteristics, the relationship between specific cell types and the three-dimensional morphology of the surface to which they are attached is poorly understood. This is particularly true for glomerular podocytes -- the gatekeepers of glomerular filtration -- which completely enwrap the glomerular basement membrane with their primary and secondary ramifications. Nanotechnologies produce biocompatible materials which offer the possibility to build substrates which differ only by topology in order to mimic the spatial organization of diverse basement membranes. With this in mind we produced and utilized rough and porous surfaces obtained from silicon to analyze the behavior of two diverse ramified cells: glomerular podocytes and a neuronal cell line used as a control.

Proper differentiation and development of ramifications of both cell types was largely influenced by topographical characteristics. Confirming previous data, the neuronal cell line acquired features of maturation on rough nanosurfaces. In contrast, podocytes developed and matured preferentially on nanoporous surfaces provided with grooves, as shown by the organization of the actin cytoskeleton stress fibers and the proper development of vinculin-positive focal adhesions.

On the basis of these findings we suggest that *in vitro* studies regarding podocyte attachment to the glomerular basement membrane should take into account the geometrical properties of the surface on which the test are conducted because physiologic cellular activity depends on the three-dimensional microenvironment.

Keywords: podocytes, neurons, nanotechnology, basement membrane, differentiation, adhesion

Running header: Glomerular podocyte differentiation *in vitro*

Introduction

Cell culture studies remain an invaluable tool for understanding cell properties and molecular mechanisms of cell damage. However, traditional two-dimensional cell cultures poorly replicate the complex *in vivo* cell-matrix interactions in different tissues. This is especially true for ramified cells because the formation of precise cell ramifications is essential to convey appropriate signals in specific tissue microenvironments. Therefore, three-dimensional (3D) cell cultures are becoming a gold standard for *in vitro* studies and have been recently facilitated by rapidly evolving nanotechnologies which create different 3D surfaces by modifying existing biocompatible materials, such as silicon.[1,2] For instance, cultured neurons have been tested on different nanosurfaces by several investigators.[3,4] Structured materials which facilitate dendrite development, adhesion, and signalling may promote better understanding of neuronal repair from pathological conditions and present novel therapeutic strategies.[5,6]

Another example of the ramified cell is the glomerular podocyte. In contrast to neuronal dendrites, podocyte ramifications intertwine among themselves and organize a web that completely envelops the external side of the glomerular capillary, thus providing the morphological basis of glomerular filtration barrier function. Adhesion to the glomerular basement membrane (GBM) is a prerequisite of healthy podocytes; detachment from the GBM and loss of podocytes in the urine is a common finding in glomerular diseases.[7-9] Despite a growing interest in potential therapeutic strategies to avoid podocyte detachment, there is incomplete knowledge of the dynamic mechanisms that regulate the anchorage of podocyte ramifications to the GBM[7,8,10-12] in order to maintain physiological properties and counteract the continuous mechanical stress due to the high transcapillary filtration pressure.[13]

The use of biomaterials offers a unique method to produce surfaces with different nanotopographies and those best fitting cell-specific requirements. It is well known that cells sense, communicate, and respond to signals from biomaterials and exhibit different adhesion, proliferation, differentiation, and consequently gene expression depending on matrix morphology.[2,5,14,15] The same occurs *in*

vivo, because the extracellular matrix (ECM) provides biophysical cues with its three-dimensional morphology.[16] These effects have been largely explored using neuronal cells in order to realize an optimal micro-nanometrical environment able not only to guide mature neuronal growth[17] and dendrite orientation[18], but also to drive neuronal differentiation.[5,19,20] The effect of substrate topography has been investigated at the micrometrical and nanometrical scale.[5,19,21-24] Lines 350nm wide made of polydimethylsiloxane (PDMS) increased neuronal differentiation with respect to flat controls.[5] Polyethersulfone fiber mesh, 700 nm in diameter, increased rat neuronal precursors differentiation.[19] Most of these surfaces are characterized by the presence of nano-pillars conferring a rough aspect.

Glomerular podocytes with their elongated primary and secondary projections firmly attach to the basement membrane of the capillary. Because of their extreme differentiation, these cells have been always difficult to produce and maintain in culture, and *in vitro* studies often rely on cells with a scarcely ramified morphology.

Based on these premises and on the report that nano-topographies based on silicon were effective in improving cell adhesion and differentiation of different cell types and particularly of ramified cells[25] , we decided to test this type of material on podocyte cell cultures.

In consideration of current knowledge regarding the surface of the glomerular basement membrane based on scanning electron microscopy studies [26], we designed studies to compare rough nano-materials with those possessing grooves instead of pillars and therefore presenting a porous surface on cross-section, in order to study the behavior of podocytes and identify the specific surface on which these cells better adhere and differentiate. Our results seem to demonstrate that podocytes actually recognize a specific geometric pattern which is different from the one optimal for neuronal cells, supporting the idea that precise tridimensional microarchitectures mimicking the in vivo microenvironment may provide better conditions for in vitro studies.

Material and methods

Nanopatterned substrates

Silicon substrates with surface random self-assembled tin nanoislands with median surface areas of 69 nm^2 (substrate N) and 163nm^2 (substrate F) and etched silicon nanopillars 775 nm^2 (substrate NE) and 405 nm^2 (substrate FE) were used in this study. The substrates were realized as previously reported [15]. Briefly, a distribution of self-assembled random nanoislands was obtained by controlled deposition of tin on the polished side of silicon wafers by thermal evaporation using a vacuum metallic evaporator (Balzer vacuum Chamber Evaporator). For thicknesses roughly below 20 nm, the deposited tin assembles spontaneously into nanoislands that grow and eventually merge into larger ones as the evaporation proceeds, according to the Ostwald ripening phenomenon. [27] Exploiting the formed nanoislands as protective masks, the wafers underwent a process of reactive ion etching in an STS inductively coupled plasma etcher (ICP) to transfer the pattern onto the silicon support. Mean nanofeature size and density were controlled by the thickness of deposited tin and the height of the etched pillars by the duration of ICP treatment. Residual tin after etching was removed by wet etching. Non-patterned silicon substrate was used as control.

Characteristics of nanopatterned surfaces

Representative scanning electron microscopy (SEM, Zeiss Supra 40 at 5KV) images of the substrates utilized in this study characterizing their surface topography are shown in Fig 1. Mean feature size, size distribution, random pattern, and density were quantified by 2D SEM images using image J software (http://imagej.en.softonic.com). The substrates were also characterized by atomic force microscopy (AFM, AFM NanoWizard II JPK). Computerized statistical analysis of surface roughness was calculated using the surface profile data extracted from the AFM images (Gwddyion software) and expressed as root mean square (q). Table 1 illustrates the main surface parameters in terms of amplitude of pillars and grooves and their organization. Water contact angle

measurements were obtained using a goniometer (CAM 100, KSV) equipped with a digital camera and image analysis software. Pure water was used as the wetting liquid.

All measurements were carried out in triplicate. Three random samples were observed each at three random spots for SEM, AFM and water contact angle studies.

Evaluation of protein adsorption on the different surfaces

To quantify the amount of culture medium adsorbed onto the different surfaces, each surface was immersed in F12 Hank's medium/Minimum essential medium (Sigma Aldrich, Italy) (1:1) supplemented with 15% fetal bovine serum (FBS) or bovine serum albumin (BSA 10 μg/ml) or fibronectin (5-20 μg/ml) and incubated in a 37°C humidified 5% CO_2 atmosphere for 4h. Each surface was gently rinsed with phosphate-buffered saline at room temperature; adhering proteins were desorbed by soaking the surface in 1% sodium dodecyl sulphate (SDS) for 15 min. Protein concentration in each eluate was determined using a commercially available kit (BCA assay kit, Pierce, Thermo Fischer, Italy). Experiments were run in triplicate.

Cell cultures

The protocols for isolation of rodent glomeruli and primary cells were approved by the Ethics Committee for Animal Experimentation (OPBA) of the University of Trieste (n. PO1640ZEN1) in compliance with Italian regulation (D.L.vo 26/2014).

The silicon surfaces were exposed to conventional sterilization treatment by autoclave prior to cell culture.

The SHSY-5Y human neuroblastoma cell line (IST-Istituto Nazionale per la ricerca sul cancro, Italy n.HTL95013) was cultured in a medium containing a 1:1 mixture of Eagle's minimum essential/F12 medium plus 15% FBS, 1% v/v nonessential aminoacids, 1% v/v glutamine and 1%

v/v penicillin/streptomycin (all from Euroclone S.p.a, Italy, Milano). For the differentiation experiments the concentration of FBS was 10% in accordance with Constantinescu et al. [28]

For primary podocyte cultures, glomeruli from healthy two-month-old male Sprague Dawley rats and C57BL6 mice were isolated by sieving, seeded in culture flasks pre-coated with collagen IV and covered by medium containing Dulbecco's modified Eagle/F12 medium (DMEM/F12) supplemented with 10% FBS, 5 µg/ml transferrin, 10^{-7}M hydrocortisone, 5 ng/ml sodium selenite, 0.12 U/ml insulin, 100 µg/ml penicillin, 100 µg/ml streptomycin, 2 mM L-glutamine (all from Sigma-Aldrich, Italy, Milano). After 10 days first passage podocytes were separated from glomeruli by an additional sieving through a 40 µm mesh (BD Falcon, Bioscientifica S.r.l, Italy) and seeded onto the nanosurfaces or on plastic. Cell characterization was performed by immunofluorescence and RT-PCR for the podocyte markers nephrin, podocin, and WT-1 (Santa Cruz, DBA Italia s.r.l; Life Technologies, Italy, Milano).

A human immortalized podocyte cell line was obtained by infection of primary cultures with a hybrid Adeno5/SV40 virus as previously described and characterized [29] and cultured in DMEM containing 25 mM glucose, 10% inactivated FBS, 100 U/ml penicillin, and 100 µg/ml streptomycin at 37°. All cell types were seeded on the nanosurfaces or on plastic coverslips at a density of $8x10^3$ cell/cm^2.

Evaluation of nanosurface biocompatibility

The biocompatibility of the different surfaces was assessed from 1 to 5 days of culture on SHSY-5Y cells by quantifying cell toxicity and metabolic activity. The degree of cell toxicity was correlated to the production of lactate dehydrogenase (LDH) measured by an assay kit (BioVision Prod., Mountain View, CA, USA) according to manufacturer instructions; 1% Triton X-100 damaged cells were utilized as positive control. Metabolic activity was determined by the MTT (3-(4,5-dimethylthiazol-2-yl)-2,5-diphenyl-tetrazolium bromide) test (Sigma Aldrich, Italy), conducted

according to standard procedures. Cell differentiation was achieved by adding 10 µM all-trans-retinoic acid (RA; Sigma Aldrich, Italy), as described. [30,31]

Cell observation

The physical characteristics of the silicon surfaces made it impossible to use standard microscopy to examine cellular morphology. To overcome this problem, we utilized Dil staining and scanning electron microscopy (SEM).

Dil (1,1'-Dioctadecyl-3,3,3',3'-Tetramethylindocarbocyanine Perchlorate, Molecular Probes, Thermo Fischer Scientific, Italy), a lipophilic dye that becomes fluorescent when incorporated into the cell membrane, was added (1ug/ml) to the medium 40 minutes before cell fixation; after extensive washing with phosphate buffer, cells were fixed in 4% paraformaldehyde.

For SEM examination, cells were fixed in 2,5% glutaraldehyde in 0,2M sodium cacodylate buffer at pH 7.4 and post-fixed in 2% OsO_4 in 0.1 M sodium cacodylate buffer at pH 7.4, dehydrated in a graded ethanol series and dried in hexamethyldisilazane. The samples were then sputter-coated with gold (Edwards S150A sputter coater) and observed under a XL30 Philips microscope. All reagents and grids for electron microscopy were from Electron Microscopy Sciences (Società Italiana Chimici, Italy).

Analysis of cell proliferation and differentiation

To measure the effect of different surfaces on cell differentiation, BrdU (Bromodeoxyuridine, BD Bioscience San Diego, US) incorporation and neurite length were analyzed at day 5 of neuronal cell culture. Cell count was performed by DAPI staining using 10 fields at low (50X) magnification whereas the analysis of circularity was performed by analyzing higher magnification images (400x; 20 fields). Circularity was calculated with Image J software, utilizing a macro that assigns the value of 1.0 to indicate a perfect circle, and values progressively approaching 0.0 to indicate an increasingly elongated polygon.

Cell cycle phase evaluation and BrdU incorporation were performed as described [32], and cells were analyzed by flow cytometry (FACS canto, Becton Dickinson, DIVA software). Image J software was used to measure the length of individual neurites in 10 images for each experiment using a magnification of 100X; for this analysis the cells were stained with DiL. All experiments were performed in triplicate.

Gene expression study

Total RNA was isolated from cells using the Invitrogen Pure Link TM Micro-to-midi Total RNA Purification System and its concentration was determined by Nanoquant (Tecan s.r.l, Italy). One microgram of total RNA was reverse transcribed using MMLV reverse transcriptase (Applied Biosystems, for Life Technologies, Italy) and utilized for semi-quantitative Real Time RT-PCR (QRT-PCR), as described. [33]

Human primers were the same as described by Constantinescu et al. [28] Human GAPDH was utilized as house-keeping gene with the following primers: *5′*-CCCATCACCATCTTCCAGGAG-*3′* (forward) and *5′*- CTTCTCCATGGTGGTGAAGACG-*3′* (reverse) (NM_002046.5).

Mouse primers were the following: MAP2 5'-AAGTCACTGTGGAATAAGC-3' (forward); 5'-CTCTGCGAATTGGTTCTG-3' (reverse) (NM_001039934.1)); β-tubulin III 5'-GCCTCCTCTCACAAGTATG-3' (forward) and 5'-CTCCGTATAGTGCCCTT-3' (reverse) (NM_023279.2); Tau 5'-CAAGACCAA GAAGGAGACATGGAC-3' (forward); 5'-CACACGAGCTTGAGTCACATGC-3' (reverse) (M18776.1) ; GAPDH *5′*-AAATGGTGAAGGTCGGTGTG-*3′* (forward); *5′*- TGAAGGGGTCGTTGATGG-*3′* (reverse) (GU214026.1).

Immunofluorescence staining

An indirect immunofluorescence method was utilized on cells fixed in paraformaldehyde. The primary antibodies were: rabbit anti-MAP2 (Merck Millipore, Italy), rabbit anti-vinculin (Sigma-

Aldrich, Italy), rabbit anti-β tubulin III (Sigma-Aldrich, Italy). Alexa Fluor 488 donkey anti-rabbit (Invitrogen) was applied as secondary antibody (Invitrogen, Thermo Fisher Scientific) and DAPI utilized as nuclear counterstain. F-actin was detected by phalloidin-FITC or phalloidin-rhodamine (Sigma-Aldrich, Italy). Samples were observed by fluorescence microscopy (Leica Microsystem Gmbh, Germany). Nuclei were stained with DAPI (4',6-diamidino-2-phenylindole; Sigma Aldrich,Italy).

Data analysis

All experiments were carried out in triplicate, and statistical analysis was performed using JMP 10 (Statistical Discovery from SAS; USA) software. Data are shown as mean ± standard error (SE). Where indicated, differences among groups was evaluated by ANOVA and judged as significant when p-value <0.05.

Results

Characteristics of nanopatterned surfaces

As shown in Fig 1, two rough surfaces (F and N) and two porous surfaces (FE and NE) were utilized in this study. Representative images of these nanostructured surfaces and their characterization by SEM, AFM, and water contact angle are reported in Figure 1.

Table 1 illustrates the main parameters of all surfaces in terms of amplitude of pillars and grooves and their organization.

The water drop contact angle demonstrated lower values for the porous surfaces FE and NE as compared to the rough surfaces F and N, indicating higher wettability of FE and NE substrates, similar to that of collagen (Fig 2a).

In addition, all nanosurfaces adsorbed significantly more medium components and more BSA than plastic and unpatterned silicon (Fig 2b), though without significant differences among themselves. Instead, at the used dosages, we were not able to identify any adsorbed fibronectin on any surfaces.

Evaluation of nanosurface biocompatibility

Previous studies have shown that SHSY-5Y cells differentiate towards a neuronal cell phenotype after 5 days of incubation with retinoic acid (RA). [28] In the current study the cell line grown on flat silicon (Si-Ctrl) and on nanopatterned surfaces demonstrated significantly lower LDH production than cells grown on plastic (Fig 3a) and showed increased metabolic activity which, however, did not reach the level of cells grown on plastic and resembled more the level of those exposed to RA (Fig 3b).

SHSY-5Y behavior on nanosurfaces

Beta tubulin III immunostaining was used to analyze the cellular morphology on nontransparent surfaces as described by Qi et al, (2013) [34]. As expected, RA treatment caused elongation of the cell body and extension of multiple ramifications (Fig 4g). In the absence of RA, cells seeded on plastic (Fig 4a), on non-patterned silicon (Si-Ctrl) (Fig 4b) or on the porous materials FE (Fig 4c) and NE (Fig 4d) remained undifferentiated. In contrast, the presence of rough nanosurfaces (F and N) alone stimulated cell differentiation (Fig 4 e-f) and cells seeded on the N rough material achieved ramification lengths comparable to that obtained by RA (Fig 4f). The parallel nuclear elongation on the F and N surfaces (4 m-n, p) associated with the cytoskeletal changes support the presence of cell differentiation towards a neuronal phenotype that was comparable to RA treatment (4o-p).

Neuronal differentiation induced by RA corresponds to a reduction of cell proliferation[30]. Cell numbers comparable to RA treatment were obtained by growing cells onto the N surface (Fig 4q). Although BrdU incorporation showed an insignificant reduction of cell proliferation (Fig 4k), cells

seeded on the N rough material achieved ramification lengths comparable to that obtained by RA (Fig 4i).

Expression studies on SHSY-5Y cells

As shown by Constantinescu and coworkers [28], once differentiated, SHSY-5Y cells express cytoskeletal and neurotransmitter markers typical of dopaminergic neurons. Accordingly, after five days of culture on rough nanosurfaces, microtubule-associated protein 2 (MAP2) expression was higher compared to other culture conditions and similar to RA treated-cells (Fig 5a). Immunofluorescence showed appropriate protein localization on cell ramifications (Fig 5c). On the contrary, cells grown on porous surfaces expressed the molecule mainly in a perinuclear location.

Confirming previous data [28,35], neurotransmitter expression changes were not evident after five days of culture (Fig 5b), but required ten days to become statistically significant (Fig 5d), particularly those of neurogenin and tyrosine hydroxylase (TH) which suggest a shift towards a dopaminergic phenotype [36]. On the other hand, at the same time point we no longer observed significant differences in expression of cytoskeletal molecules (Fig 5e), suggesting that modifications of the cytoskeleton are first required in order to achieve a complete differentiation.

Interestingly, all cells grown on nanopatterned materials showed a different gene expression as compared to cells seeded on plastic, suggesting recognition of and reactivity to uneven surfaces.

Podocyte behavior on nanosurfaces

In traditional two-dimensional cell culture conditions, podocytes best develop when grown on collagen-coated plastic. This characteristic was confirmed in our experiments; Dil staining showed that podocytes remained undifferentiated and cuboid on uncoated plastic (Fig 6a2) whereas on collagen-coated plastic they acquired a differentiated, arborized phenotype (Fig 6g2; Fig 7e).

In contrast to SHSY-5Y cells, an undifferentiated podocyte pattern was observed on the rough nanosurfaces F and N (Fig 6 c2-d2; Fig 7a-b), whereas porous materials (FE and NE) induced a

differentiated morphology characterized by elongation of the cell body and the appearance of an arborized phenotype (Fig 6 e2-f2, 6i; Fig 7c-d). Evaluation of morphology by SEM (Fig 7f-j) and proliferation indexes (Fig 6h) confirmed these observations. Accordingly, the presence of stress fibers typical of differentiated podocytes was observed in cells grown on porous surfaces (Fig 6e1, 6f1) as well as on collagen-coated plastic (Fig 6g1) whereas peripheral bundles of subcortical actin predominated in cells adherent to rough surfaces or uncoated plastic (Fig 6c1,d1,a1). The observed cytoskeletal changes also involved the formation of focal adhesions, as shown by vinculin abundance and localization that paralleled actin changes (Fig 8). Forty-eight hours were sufficient for human podocytes to show a peripheral punctated vinculin pattern co-localizing at the tip of stress fibers (Fig 8a). At the same time point, both stress fibers and vinculin expression appeared decreased in presence of rough materials (Fig 8b) but were increased in cells grown on porous nanosurfaces (Fig 7c).

At day five of culture on rough surfaces, vinculin expression was mostly cytoplasmic and the pattern of expression suggested intramolecular head to tail binding typical of the inactive form of the molecule (Fig 9a). In contrast, porous materials influenced the punctated expression of active vinculin co-localizing with actin stress-fibers at peripheral focal contacts (Fig 9 b-d).

Expression studies on podocytes

Podocytes and neuronal cells share numerous lineage-restricted molecules, including cytoskeletal proteins such as MAP2 and Tau [12,37] and synaptic molecules such as synaptophysin. [38] Increased MAP2 and Tau (Fig 10 a) as well as β tubulin III (Fig 10 c) were observed at day five of culture onto both porous surfaces NE and FE. No differences were found in synaptophysin expression.

Discussion

Cells interact with the extracellular matrix in a complex manner that comprises molecular as well as geometrical cues. [39-41] Cell-matrix molecular interactions have been revealed by numerous *in vitro* and *in vivo* experimental studies, but the relationship between specific cell types and the geometry of the surface to which they attach remains mostly to be analyzed. Nanotechnologies are useful for for these studies because of the unique opportunity to utilize and modify diverse biocompatible materials and build substrates which differ only by topology. Basement membranes are not the same in all tissues but differ in the geometry of 5-200 nm size pits, pores, protrusions, and fibers, so that nanostructured biomaterials can mimic the spatial organization and separation distances which are characteristic of each specific basement membrane.[42]

In the present study rough and porous surfaces in which pillars and grooves are separated by a distance less than 58 nm, which corresponds to the maximum distance required for correct establishment of focal adhesions [25,43], were obtained from silicon and compared not only to flat silicon but also to plastic surfaces which are routinely utilized for traditional two-dimensional cell cultures.

Although flat silicon was in itself advantageous as compared to plastic in terms of biocompatibility, it was not sufficient to influence cell differentiation, supporting the concept that cells need more specific stimuli from their microenvironment. In addition, all nanopatterned surfaces were found to absorb more medium components than flat materials, suggesting a diverse biomolecular relationship with the contacting cells.

The SH-SH5Y neuronal cell line was utilized as a control because of its known sensitivity to environmental stimuli.[44] Our experiments confirmed the ability to sense surface roughness and to respond with changes in adhesion, development and function. [6] In addition, our studies indicate that the density of pillars is relevant to acquire enhanced differentiation of the cell line because the N material, characterized by smaller and nearer pillars, resulted to be the optimal environment to favor cell differentiation. Therefore, this specific geometry mimics the environment required for

dopaminergic neuronal cells, which show similar changes as those obtained with retinoic acid routinely utilized to obtain cell differentiation in two-dimensional cell cultures. [28,30,31,45,46]

Perhaps not surprisingly, a completely different geometric nanoporous surface nurtured primary rodent and human podocytes, on which arborized cell processes were formed similarly to those traditionally obtained by collagen coating. In this sense podocytes, despite the presence of numerous ramifications, display a similar behavior to that of other epithelial cell types whose attachment and spreading seem to be discouraged by rough surfaces [47,48] and facilitated instead by nanoporous materials. [49] This behavior was not unexpected as it indirectly confirms what is known about the geometry of the GBM surface obtained by scanning electron microscopy studies performed after freeze-fracture procedures optimized to get a view of the GBM itself. From these analyses, the GBM appears indeed porous, which is required for the primary filtering function of the glomerular capillary. [26,50-54]

During embryological development, podocyte precursors display a cuboidal shape and subsequently develop primary major processes and secondary foot processes, which intertwine among themselves and completely enwrap the GBM. Adhesion of podocyte processes to the GBM involves a focal integrin-mediated adhesion structure described as a "cellular sensing machinery" [6] formed by vinculin, talin and paxillin, which direct focal adhesion assembly by linking actin to transmembrane integrins.[2] Similarly, *in vitro* immature podocytes have a cobblestone shape, and maturation proceeds after firm cellular adhesion with the formation of ramifications. As confirmed by our results, these events are accompanied by profound remodeling of the actin cytoskeleton[55], with formation of stress fibers. As regarding adhesion, both rough and porous materials were initially able to induce immature vinculin expression, as shown by a homogeneous distribution of the molecule in the cytoplasm. However, only porous surfaces allowed the formation of mature large and stable punctate focal contacts which appeared after five days of incubation and co-localized with actin filaments. In contrast, at the same time point only inactive vinculin was present in cells seeded on rough nanosurfaces, demonstrating the absence of mature focal adhesions.[56] These

findings also suggest that before structuring permanent adhesions, podocytes test the microenvironment forming labile and soft interactions, a behavior which is likely relevant to find the exact orientation of the cell body and of cell ramifications on the preferred surface and is followed by the establishment of mature and stable contacts.

Several studies have demonstrated a series of analogies between podocytes and neuronal cells, particularly concerning the organization of the cytoskeleton and the formation of cell ramifications. [10-12,57] Our experiments confirm these results, showing that differentiation of both cell types starts from cytoskeletal changes expressed, for instance, as an increase in MAP2 expression. MAP2 belongs to the class of microtubule-associated proteins, an abundant group of cytoskeleton components predominantly expressed in neurons. In these cells microtubules are essential to formation and maintenance of neurites, and specifically MAP-2 contributes to microtubule stabilization by tubulin polymerization in association with Tau[11]. Additional evidence also demonstrated the role of MAPs in bridging microtubules and actin-microfilaments in several cell types.[58]A significant up-regulation of MAP2 expression has been described during neuronal differentiation of human mesenchymal stem cells in the presence of nanostructured surfaces with or without retinoic acid as compared to flat surfaces[5]. In our hands, the cytoskeletal changes may represent a prerequisite for the subsequent increased expression of dopaminergic neuronal markers which confirm the complete differentiation [28].

Similarly to neuronal cells, mature podocytes show major processes which are microtubule-based cellular extensions interwoven with intermediate filaments and secondary foot processes containing a microfilament-based contractile apparatus composed of actin, myosin-II, a-actinin, talin, and vinculin.[10] Neuronal MAPs have been shown to promote microtubules assembly in podocytes [10,11]; in particular MAP2 and Tau were both demonstrated in podocytes [10-12] suggesting a role in bridging microtubules and actin microfilaments, which are essential to cellular maturation. The role of microtubules in podocyte development is confirmed by our results showing increased expression of microtubule-related molecules including MAP2, Tau and the neuronal tubulin isoform β tubulin III,

which are particularly induced by the NE surface, characterized by closer and more regularly spaced grooves than the FE material. IF analysis of β tubulin III not only showed its increased expression, but also demonstrated the preferential longitudinal orientation of the molecule when cells were grown on the NE surface.

As summarized in Fig 11, the present study shows that two different types of ramified cells -- neuronal cells and podocytes--are able to recognize and firmly attach to substrates according to the precise geometry which better reproduces the *in vivo* microenvironment. Culture studies specifically associating the preferred molecular and topographical cues for any cell types seem to be the best way to improve validity and reproducibility of in *vitro* findings.

The hallmark of numerous proteinuric renal diseases is podocyte injury characterized by foot process effacement, dedifferentiation and detachment from the basement membrane with migration or loss. The results of this study seem to suggest that extracellular topographic cues play a critical role in initiation and maintenance of cell adhesion and phenotype fate. Importantly, the control of this cell behavior can be achieved by modifying the pattern of the topographic characteristics. Thus, we propose a simple, robust and accessible biomimetic nanostructured platform with the potential to model *in vitro* podocyte cell biology and pathology, which may be applicable also to podocyte-endothelial co-culture systems[59], virtually recapitulating the glomerular filtration barrier. Critically, this may find utility in the investigation and further understanding of molecular pathways at the heart of podocyte well-being and injury.

Summary and conclusion

In this study we present a series of experiments conducted on podocytes and neuronal cells, two cell types that, despite a number of commonalities, are very different in their behavior and function and are connected, in vivo, to different types of extracellular matrix. Our results seem to show that also in vitro these cells behave differently in that they recognize and grow on specific tridimensional substrates. The importance of geometrical cues, and a better reproduction of in vivo characteristics, are highlighted by our data and can offer a starting point for future in vitro studies.

Acknowledgments

This work was supported by ‘‘Fondazione la Nuova Speranza ONLUS - Lotta alla Glomerulosclerosi Focale’’, Rho (Mi). Funding was received also from ‘‘Fondazione Benefica Kathleen Foreman Casali’’, Trieste. Dr. Tonon is presently the recipient of a Telethon Foundation research contract.

Disclosure

The authors report no conflicts of interest in this work.

Figure legends

Fig 1: Features of nanosurfaces.

(a) SEM images clearly show the aspects of the different nanosurfaces utilized in the study. F and N surfaces are characterized by pillars whereas FE and NE surfaces show grooves. bar=20 nm;

(b) Graph plot of the frequency distribution of surface area of substrate nanostructures sampled with 50 nm^2 area classes;

(c) AFM topography profiles.

Abbreviations: SEM, scanning electron microscopy; AFM, atomic force microscopy.

Fig 2: Water drop contact angle and protein absorption of nanosurfaces.

(a) Representative images of water drop contact angle of the surfaces included in this study. The Table shows the measured values for each surface.

(b) After four hours incubation, patterned surfaces show higher protein absorption from the whole medium (upper graph) and higher BSA adsorption (lower graph) than plastic and non-patterned silicon. The difference with plastic is statistically significant for NE, N, and F surfaces.

Fig 3: Nanosurface biocompatibility

(a) LDH levels are compared to those produced after cell damage with Triton, taken as 100%. SHSY-5Y cells after 1 (black bars) and 3 days (light gray bars) of culture display LDH levels reduced by 40% from baseline. At five days (gray bars) silicon surfaces and treatment with RA further diminish LDH release, which becomes statistically significant in comparison to the same time point on plastic.

(b) MTT assay confirms that cells are healthy on all surfaces and at any time points. In addition, the test shows a statistically significant difference at five days between cells grown on plastic and those treated with RA or seeded on the N surface.

Results are expressed as mean ± SE. *p<0.01 compared to plastic and **p<0.001 compared to plastic.

Abbreviations: LDH, lactate dehydrogenase; RA, retinoic acid; MTT, 3-(4,5-dimethylthiazol-2-yl)-2,5-diphenyl-tetrazolium bromide; Si_crtl, unpatterned silicon surface.

Fig 4: Behavior of SHSY-5Y cells on different nanosurfaces.

SHSY-5Y cells were immunostained with anti β-tubulin III (green) and nuclei counterstained with DAPI (blue). The cells have an undifferentiated morphology, represented by short ramifications, when grown on plastic (a), non-patterned silicon (b) and porous materials FE (c) and NE (d). A differentiated, elongated phenotype with long cell projections is present on rough materials F (e) and N (f), as well as after RA treatment (g).

The graph in the panel (h) shows the results of measurement of cell ramification length, that resulted significantly higher in cells grown on the surface N and after RA treatment.

By evaluation at higher magnification, the nuclear shape appears mostly rounded in cells grown on plastic (i), unpatterned silicon (j) or on the porous materials FE (k) and NE (l), whereas adherence to the rough surfaces F (m) and N (n) as well as exposure to RA (o) seem to induce nuclear elongation.

(p) The graph shows the results obtained by measurement of nuclear circularity, which is the highest in cells cultivated on unpatterned silicon and the lowest in cells grown on rough surfaces or exposed to RA.

(q) In the histogram the cell number is expressed as percentage of values shown by cells grown on plastic, taken as 100%. A statistically significant decrease is shown by cells grown on the rough surface N, as well as after RA treatment.

(r) After five days of culture, only cells treated with RA display a statistically significant lower BrdU incorporation than cells grown on plastic.

Scale bars = 50um. Panels h, p, q, r: Results are expressed as mean ± SE. *p<0.01; **p<0.001; ***p<0.0001, all compared to plastic.

Abbreviations: DAPI, 4',6-diamidino-2-phenylindole; RA, retinoic acid; BrdU, Bromodeoxyuridine; Si-ctrl, unpatterned silicon surface.

Fig 5: Expression studies on SHSY-5Y cells.

(a) Among the cytoskeletal components Tau (red bars), beta-tubulin III (green bars), and MAP-2 (violet bars), a significant increase of MAP2 expression is shown at five days of culture by cells grown on the rough surfaces N and F, as well as by cells stimulated with RA.

(b) MAP-2 staining on SHSY-5Y cells shows the molecule barely expressed by cells grown on plastic (first row, left panel), non-patterned silicon (Si-ctrl, first row, middle panel), and the porous surface NE (first row, right panel). MAP2 expression along cell processes can be detected in cells grown on the surface N (second row, left panel), and better appreciated at higher magnification of the punctated square area (second row, middle panel), similar to what is observed in cells treated with RA (second row, right panel). Scale bars = 50 um.

(c) The expression of molecules related to neurotransmission, including synaptophysin (blue bars), neurogenin (red bars), thyrosine hydroxylase (TH, green bars), and DDR2 (violet bars), is not significantly modified at five days of culture.

(d) At ten days, expression of synaptophysin (blue bars) and TH (green bars) is significantly increased in cells grown on the N surface, whereas at this time point the difference among cytoskeletal molecules (e) is no longer present.

*p<0.01 and **p<0.001 compared to plastic.

Abbreviations: RA, retinoic acid; Si-ctrl, unpatterned silicon surface.

Fig 6: Morphology of primary mouse podocytes.

Representative F-actin (left panels a1-g1) and Dil staining (right panels a2-g2) images of primary mouse podocytes after five days of culture. Cobblestone phenotype and peripheral subcortical actin pattern are shown by cells grown on uncoated plastic (a1-2), non-patterned silicon (b1-2), and the rough surfaces F (c1-2) and N (d1-2). In contrast, cells seeded on the porous surfaces FE (e1-2) and NE (f1-2) resemble differentiated podocytes grown on collagen-coated plastic (g1-2), showing elongated cell body, presence of numerous ramifications, and actin stress fibers. Scale bars = 50 um.

(h) The number of cells is significantly reduced as compared to uncoated plastic in presence of the FE and NE surfaces.

(i) The cells on NE and FE surfaces show statistically significant increase of number of projections as compared to uncoated plastic. In contrast, exposure to unpatterned silicon greatly diminishes the number of cell processes.

Results are expressed as mean ± SE. ***$p<0.0001$ and § $p<0.05$

Abbreviations: Dil 1'-Dioctadecyl-3,3,3',3'-Tetramethylindocarbocyanine Perchlorate; Si_ctrl, unpatterned silicon surface.

Fig 7: Morphology of primary rat podocytes.

Representative Dil staining (a-e) and SEM (f-j) images of rat podocytes after five days of culture on nanopatterned silicon and collagen-coated plastic. Rat podocytes did not attach to uncoated plastic or to unpatterned silicon.

A cobblestone morphology is observed when cells are seeded on the rough surfaces F (a) and N (b, f, g), whereas cells grown on FE (c) and NE (d, h, i, j) porous materials present elongated shape and are provided with ramifications, similarly to cells grown on collagen-coated plastic (e). The morphology of a podocyte ramification extending from the cell body and adhering on the porous

surface NE can be better observed by SEM at higher magnification (j). Panels a-e: scale bars = 50 um.

Abbreviations: Dil**,** 1'-Dioctadecyl-3,3,3',3'-Tetramethylindocarbocyanine Perchlorate**;** SEM, scanning electron microscopy

Fig 8: Podocyte focal adhesions and actin cytoskeleton.

Representative images of the human podocyte cell line after two days of culture. Though cells are not yet arborized, vinculin (left panels) positivity is higher in cells grown on collagen-coated plastic (a) and on NE surface (c) than in cells adherent to the N surface (c). Rhodamine-phalloidin (middle panels) confirms the preferential organization of the actin cytoskeleton in stress fibers in collagen-coated (a) and NE surface (c), whereas peripheral actin prevails in cells grown on N material (b). Merging (right panels), particularly at higher magnification, shows that vinculin co-localizes with the tip of actin filaments in a) and c).

Scale bars = 10um

Fig 9: Podocyte focal adhesions and actin cytoskeleton.

After five days of culture, the human podocyte cell line grown on N surface shows cytoplasmic vinculin with a rounded appearance, typical of the inactive molecule. In contrast, a punctated pattern is present in cells seeded on the NE material (b). Vinculin puncta of cells grown on NE surface co-localize with actin tips (c), as better observed at higher magnification (d).

Scale bars = 10 um

Fig 10: Podocyte expression changes.

At five days of culture, the human podocyte cell line (a) shows a statistically significant increase of Tau (blue bars) in cells seeded on porous surfaces. Mouse primary podocytes (b) display a significant increase of Tau (blue bars), beta-tubulin III (red bars), and MAP2 (green bars) when grown on the NE surface.

*p<0.01, and **p<0.001 compared to plastic

(c) Immunostaining shows that mouse primary podocytes display increased and more ordered positivity (along the longitudinal axis of the cell) for beta-tubulin III, when grown on collagen-coated plastic (second row, left panel) or on the NE surface (second row, right panel) than cells grown on uncoated plastic (first row, left panel) or on the N surface (first row, right panel).

Scale bars = 50 um

Fig 11: Geometry recognition differences between a neuronal cell line and podocytes.

The neuronal cell line (a) has a preference for artificial surfaces provided with pillars which promote appropriate cellular adhesion and differentiation. On the contrary, podocytes preferentially recognize grooves (b) and pores on cross-section, suggesting that this type of surface better resembles the three-dimensional surface of the glomerular basement membrane (GMB) *in vivo*, here represented in a transmission electron microscopy image of a normal rat glomerulus (c), with arrows indicating the adhesion areas between the foot processes (FP) and the GMB. Scale bar = 100 nm

Tab. 1: Characterization of nanostructured substrates used in this study

References

1. Mendes PM. Cellular nanotechnology: making biological interfaces smarter. *Chemical Society reviews.* 2013;42(24):9207-9218.
2. Lim JY, Dreiss AD, Zhou Z, et al. The regulation of integrin-mediated osteoblast focal adhesion and focal adhesion kinase expression by nanoscale topography. *Biomaterials.* 2007;28(10):1787-1797.
3. Migliorini E, Grenci G, Ban J, et al. Acceleration of neuronal precursors differentiation induced by substrate nanotopography. *Biotechnology and bioengineering.* 2011;108(11):2736-2746.
4. Fabbro A, Bosi S, Ballerini L, Prato M. Carbon nanotubes: artificial nanomaterials to engineer single neurons and neuronal networks. *ACS chemical neuroscience.* 2012;3(8):611-618.
5. Yim EK, Pang SW, Leong KW. Synthetic nanostructures inducing differentiation of human mesenchymal stem cells into neuronal lineage. *Experimental cell research.* 2007;313(9):1820-1829.
6. Brunetti V, Maiorano G, Rizzello L, et al. Neurons sense nanoscale roughness with nanometer sensitivity. *Proceedings of the National Academy of Sciences of the United States of America.* 2010;107(14):6264-6269.
7. Kriz W, Shirato I, Nagata M, LeHir M, Lemley KV. The podocyte's response to stress: the enigma of foot process effacement. *American journal of physiology. Renal physiology.* 2013;304(4):F333-347.
8. Lennon R, Randles MJ, Humphries MJ. The importance of podocyte adhesion for a healthy glomerulus. *Frontiers in endocrinology.* 2014;5:160.
9. Kriz W, Lemley KV. A potential role for mechanical forces in the detachment of podocytes and the progression of CKD. *Journal of the American Society of Nephrology : JASN.* 2015;26(2):258-269.
10. Kobayashi N, Gao SY, Chen J, et al. Process formation of the renal glomerular podocyte: is there common molecular machinery for processes of podocytes and neurons? *Anatomical science international.* 2004;79(1):1-10.
11. Kobayashi N. Mechanism of the process formation; podocytes vs. neurons. *Microscopy research and technique.* 2002;57(4):217-223.
12. Smoyer WE, Mundel P. Regulation of podocyte structure during the development of nephrotic syndrome. *Journal of molecular medicine.* 1998;76(3-4):172-183.
13. Suleiman H, Zhang L, Roth R, et al. Nanoscale protein architecture of the kidney glomerular basement membrane. *eLife.* 2013;2:e01149.
14. Bakeine GJ, Bertolotti A, Latina M, et al. Surface properties and implantation site affect the capsular fibrotic overgrowth. *J Biomed Mater Res A.* 2007;83A(4):965-969.
15. Bakeine GJ, Bertolotti A, Zennaro C, et al. Design and fabrication of large area nano-structured substrates for use in pancreatic beta-cell engineering. *Microelectron Eng.* 2009;86(4-6):1468-1472.
16. Timpl R. Macromolecular organization of basement membranes. *Current opinion in cell biology.* 1996;8(5):618-624.
17. Rajnicek A, McCaig C. Guidance of CNS growth cones by substratum grooves and ridges: effects of inhibitors of the cytoskeleton, calcium channels and signal transduction pathways. *Journal of cell science.* 1997;110 (Pt 23):2915-2924.
18. Dowell-Mesfin NM, Abdul-Karim MA, Turner AM, et al. Topographically modified surfaces affect orientation and growth of hippocampal neurons. *Journal of neural engineering.* 2004;1(2):78-90.

19. Christopherson GT, Song H, Mao HQ. The influence of fiber diameter of electrospun substrates on neural stem cell differentiation and proliferation. *Biomaterials.* 2009;30(4):556-564.
20. Lee DA, Knight MM, Campbell JJ, Bader DL. Stem cell mechanobiology. *Journal of cellular biochemistry.* 2011;112(1):1-9.
21. Markert LD, Lovmand J, Foss M, et al. Identification of distinct topographical surface microstructures favoring either undifferentiated expansion or differentiation of murine embryonic stem cells. *Stem cells and development.* 2009;18(9):1331-1342.
22. Park J, Bauer S, von der Mark K, Schmuki P. Nanosize and vitality: TiO2 nanotube diameter directs cell fate. *Nano letters.* 2007;7(6):1686-1691.
23. Meinel AJ, Kubow KE, Klotzsch E, et al. Optimization strategies for electrospun silk fibroin tissue engineering scaffolds. *Biomaterials.* 2009;30(17):3058-3067.
24. Wang G, Ao Q, Gong K, et al. The effect of topology of chitosan biomaterials on the differentiation and proliferation of neural stem cells. *Acta biomaterialia.* 2010;6(9):3630-3639.
25. Jeon H, Simon CG, Jr., Kim G. A mini-review: Cell response to microscale, nanoscale, and hierarchical patterning of surface structure. *Journal of biomedical materials research. Part B, Applied biomaterials.* 2014;102(7):1580-1594.
26. Hironaka K, Makino H, Yamasaki Y, Ota Z. Renal basement membranes by ultrahigh resolution scanning electron microscopy. *Kidney international.* 1993;43(2):334-345.
27. Rosenfeld G, Morgenstern K, Esser M, Comsa G. Dynamics and stability of nanostructures on metal surfaces. *Appl Phys a-Mater.* 1999;69(5):489-496.
28. Constantinescu R, Constantinescu AT, Reichmann H, Janetzky B. Neuronal differentiation and long-term culture of the human neuroblastoma line SH-SY5Y. *Journal of neural transmission. Supplementum.* 2007(72):17-28.
29. Doublier S, Musante L, Lupia E, et al. Direct effect of plasma permeability factors from patients with idiopatic FSGS on nephrin and podocin expression in human podocytes. *International journal of molecular medicine.* 2005;16(1):49-58.
30. Edsjo A, Holmquist L, Pahlman S. Neuroblastoma as an experimental model for neuronal differentiation and hypoxia-induced tumor cell dedifferentiation. *Seminars in cancer biology.* 2007;17(3):248-256.
31. Vesanen M, Salminen M, Wessman M, Lankinen H, Sistonen P, Vaheri A. Morphological differentiation of human SH-SY5Y neuroblastoma cells inhibits human immunodeficiency virus type 1 infection. *The Journal of general virology.* 1994;75 (Pt 1):201-206.
32. Werth D, Grassi G, Konjer N, et al. Proliferation of human primary vascular smooth muscle cells depends on serum response factor. *European journal of cell biology.* 2010;89(2-3):216-224.
33. Zennaro C, Rastaldi MP, Pascolo L, et al. Podocyte expression of membrane transporters involved in puromycin aminonucleoside-mediated injury. *PloS one.* 2013;8(6):e66159.
34. Qi L, Li N, Huang R, et al. The effects of topographical patterns and sizes on neural stem cell behavior. *PloS one.* 2013;8(3):e59022.
35. Korecka JA, van Kesteren RE, Blaas E, et al. Phenotypic characterization of retinoic acid differentiated SH-SY5Y cells by transcriptional profiling. *PloS one.* 2013;8(5):e63862.
36. Lopes FM, Schroder R, da Frota ML, Jr., et al. Comparison between proliferative and neuron-like SH-SY5Y cells as an in vitro model for Parkinson disease studies. *Brain research.* 2010;1337:85-94.
37. Shankland SJ. The podocyte's response to injury: role in proteinuria and glomerulosclerosis. *Kidney international.* 2006;69(12):2131-2147.
38. Rastaldi MP, Armelloni S, Berra S, et al. Glomerular podocytes contain neuron-like functional synaptic vesicles. *FASEB journal : official publication of the Federation of American Societies for Experimental Biology.* 2006;20(7):976-978.

39. Daley WP, Peters SB, Larsen M. Extracellular matrix dynamics in development and regenerative medicine. *Journal of cell science.* 2008;121(Pt 3):255-264.
40. Shukla A, Slater JH, Culver JC, Dickinson ME, West JL. Biomimetic Surface Patterning Promotes Mesenchymal Stem Cell Differentiation. *ACS applied materials & interfaces.* 2015. Dec 17. [Epub ahead of print] PubMed PMID: 26674708
41. Dado D, Sagi M, Levenberg S, Zemel A. Mechanical control of stem cell differentiation. *Regenerative medicine.* 2012;7(1):101-116.
42. Teixeira AI, Abrams GA, Bertics PJ, Murphy CJ, Nealey PF. Epithelial contact guidance on well-defined micro- and nanostructured substrates. *Journal of cell science.* 2003;116(Pt 10):1881-1892.
43. Cavalcanti-Adam EA, Aydin D, Hirschfeld-Warneken VC, Spatz JP. Cell adhesion and response to synthetic nanopatterned environments by steering receptor clustering and spatial location. *HFSP journal.* 2008;2(5):276-285.
44. Buttiglione M, Vitiello F, Sardella E, et al. Behaviour of SH-SY5Y neuroblastoma cell line grown in different media and on different chemically modified substrates. *Biomaterials.* 2007;28(19):2932-2945.
45. Linnala A, Lehto VP, Virtanen I. Neuronal differentiation in SH-SY5Y human neuroblastoma cells induces synthesis and secretion of tenascin and upregulation of alpha(v) integrin receptors. *Journal of neuroscience research.* 1997;49(1):53-63.
46. Yu J, Gonzalez S, Martinez L, Diez-Pardo JA, Tovar JA. Effects of retinoic acid on the neural crest-controlled organs of fetal rats. *Pediatric surgery international.* 2003;19(5):355-358.
47. Hamilton DW, Chehroudi B, Brunette DM. Comparative response of epithelial cells and osteoblasts to microfabricated tapered pit topographies in vitro and in vivo. *Biomaterials.* 2007;28(14):2281-2293.
48. Baharloo B, Textor M, Brunette DM. Substratum roughness alters the growth, area, and focal adhesions of epithelial cells, and their proximity to titanium surfaces. *J Biomed Mater Res A.* 2005;74(1):12-22.
49. Leong MF, Chian KS, Mhaisalkar PS, Ong WF, Ratner BD. Effect of electrospun poly(D,L-lactide) fibrous scaffold with nanoporous surface on attachment of porcine esophageal epithelial cells and protein adsorption. *J Biomed Mater Res A.* 2009;89(4):1040-1048.
50. Kubosawa H, Kondo Y. Quick-freeze, deep-etch studies of renal basement membranes. *Microscopy research and technique.* 1994;28(1):2-12.
51. Shirato I, Tomino Y, Koide H, Sakai T. Fine structure of the glomerular basement membrane of the rat kidney visualized by high-resolution scanning electron microscopy. *Cell and tissue research.* 1991;266(1):1-10.
52. Takami H, Naramoto A, Shigematsu H, Ohno S. Ultrastructure of glomerular basement membrane by quick-freeze and deep-etch methods. *Kidney international.* 1991;39(4):659-664.
53. Reale E, Luciano L, Kuhn KW, Stolte H. Morphological and functional aspects of the glomerular basement membrane. *Basic and applied histochemistry.* 1979;23 Suppl:5-11.
54. Wheeler EE, Herdson PB. Freeze fracturing and freeze drying of renal tissue for scanning electron microscopy. *American journal of clinical pathology.* 1973;60(2):229-233.
55. Faul C, Asanuma K, Yanagida-Asanuma E, Kim K, Mundel P. Actin up: regulation of podocyte structure and function by components of the actin cytoskeleton. *Trends in cell biology.* 2007;17(9):428-437.
56. Humphries JD, Wang P, Streuli C, Geiger B, Humphries MJ, Ballestrem C. Vinculin controls focal adhesion formation by direct interactions with talin and actin. *The Journal of cell biology.* 2007;179(5):1043-1057.
57. Li M, Armelloni S, Zennaro C, et al. BDNF repairs podocyte damage by microRNA-mediated increase of actin polymerization. *The Journal of pathology.* 2015;235(5):731-744.

58. Sanchez C, Diaz-Nido J, Avila J. Phosphorylation of microtubule-associated protein 2 (MAP2) and its relevance for the regulation of the neuronal cytoskeleton function. *Progress in neurobiology.* 2000;61(2):133-168.
59. Li M, Corbelli A, Watanabe S, et al. Three-dimensional podocyte-endothelial cell co-cultures: Assembly, validation, and application to drug testing and intercellular signaling studies. *European journal of pharmaceutical sciences : official journal of the European Federation for Pharmaceutical Sciences.* 2016;86:1-12.

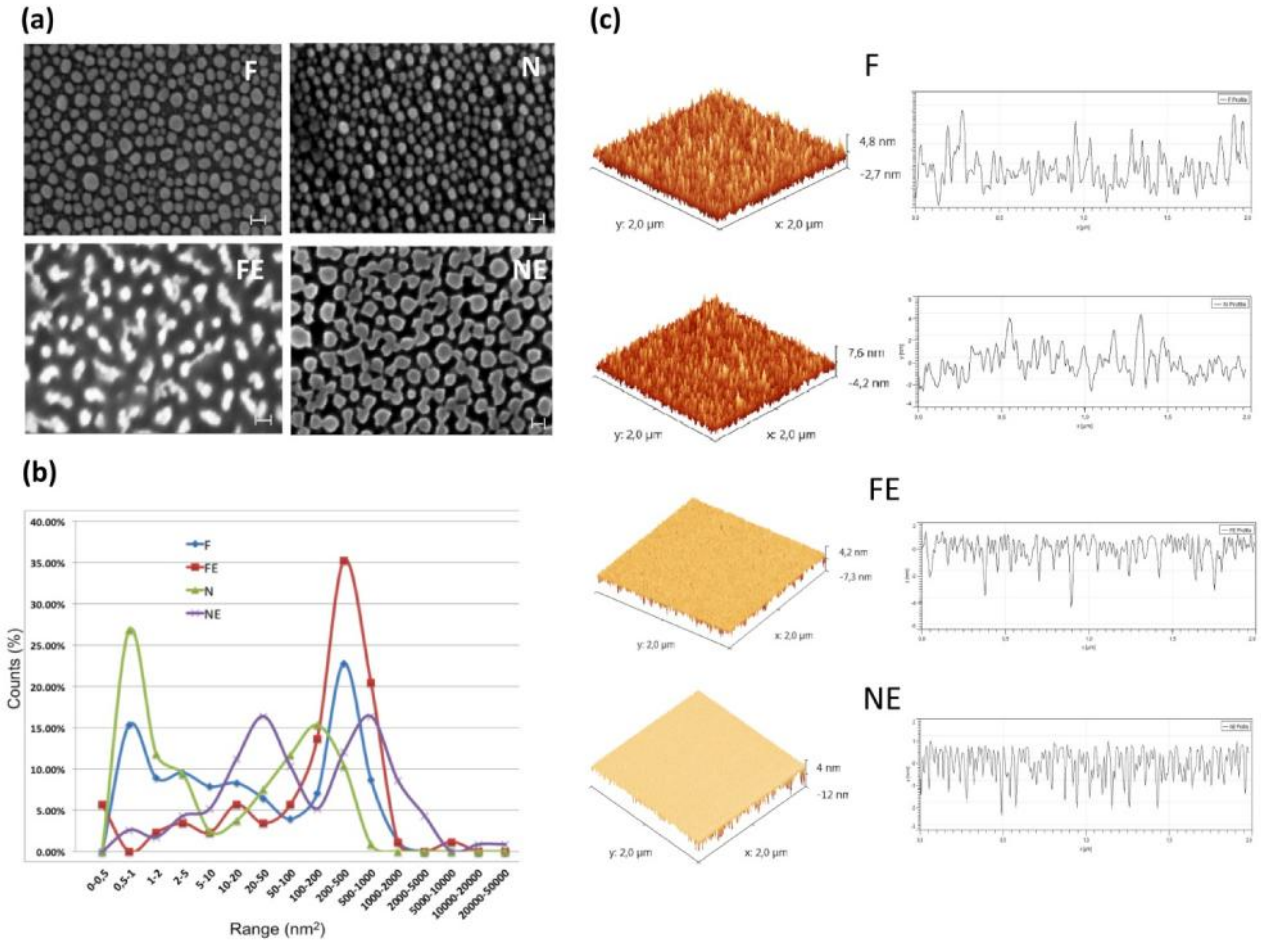
(a)
F
N
FE
NE
(b)
Counts (%)
Range (nm²)
F
FE
N
NE
(c)
F
4,8 nm
-2,7 nm
y: 2,0 µm
x: 2,0 µm
7,6 nm
-4,2 nm
FE
4,2 nm
-7,3 nm
NE
4 nm
-12 nm

Fig 1

(a)

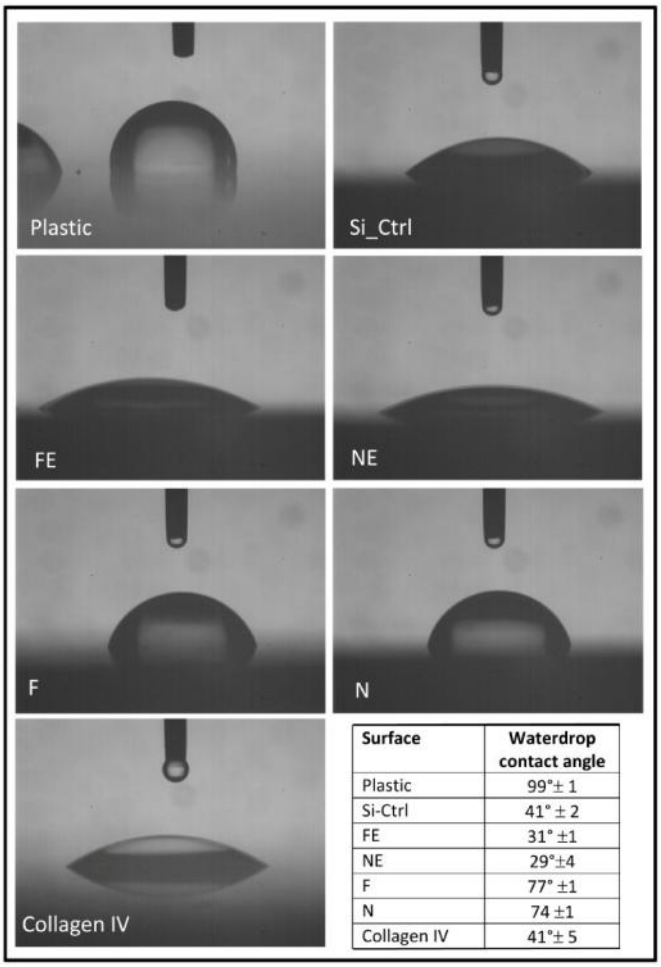

Surface	Waterdrop contact angle
Plastic	99°± 1
Si-Ctrl	41° ± 2
FE	31° ±1
NE	29°±4
F	77° ±1
N	74 ±1
Collagen IV	41°± 5

(b)

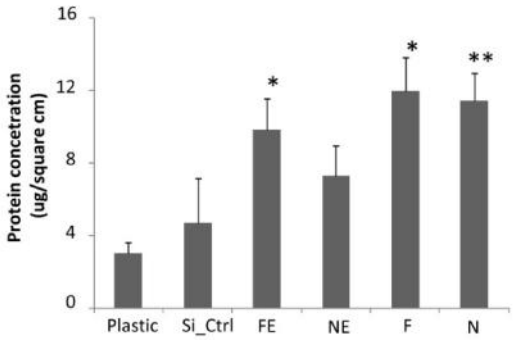

(c)

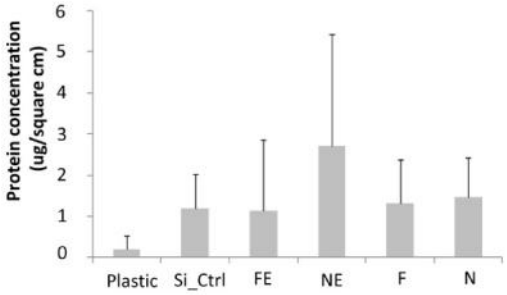

Fig 2

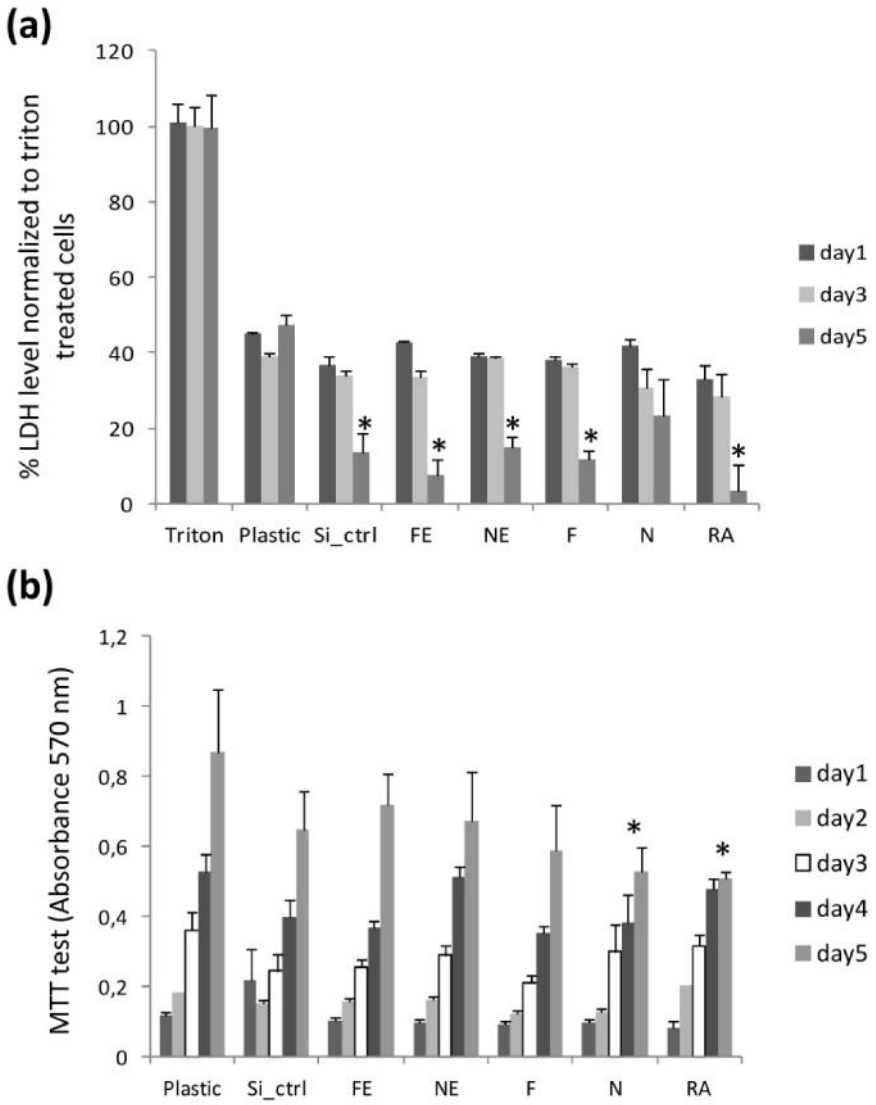
(a)
% LDH level normalized to triton treated cells
120
100
80
60
40
20
0
Triton
Plastic
Si_ctrl
FE
NE
F
N
RA
day1
day3
day5
(b)
MTT test (Absorbance 570 nm)
1,2
1
0,8
0,6
0,4
0,2
0
Plastic
Si_ctrl
FE
NE
F
N
RA
day1
day2
day3
day4
day5

Fig 3

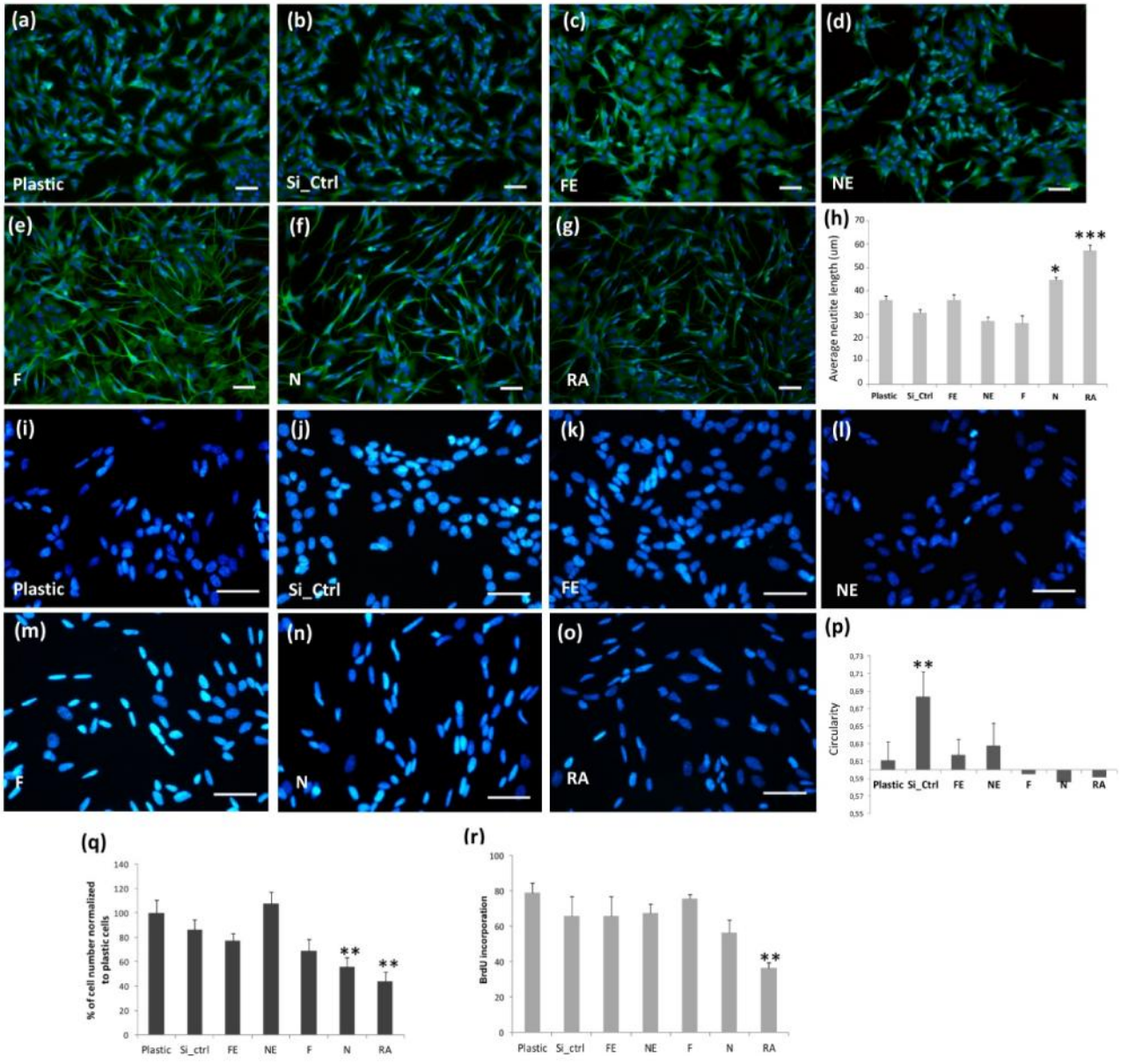
(a)
Plastic
(b)
Si_Ctrl
(c)
FE
(d)
NE
(e)
F
(f)
N
(g)
RA
(h)
Average neutite length (um)
Plastic Si_Ctrl FE NE F N RA
(i)
Plastic
(j)
Si_Ctrl
(k)
FE
(l)
NE
(m)
F
(n)
N
(o)
RA
(p)
Circularity
Plastic Si_Ctrl FE NE F N RA
(q)
% of cell number normalized to plastic cells
Plastic Si_ctrl FE NE F N RA
(r)
BrdU incorporation
Plastic Si_ctrl FE NE F N RA

Fig 4

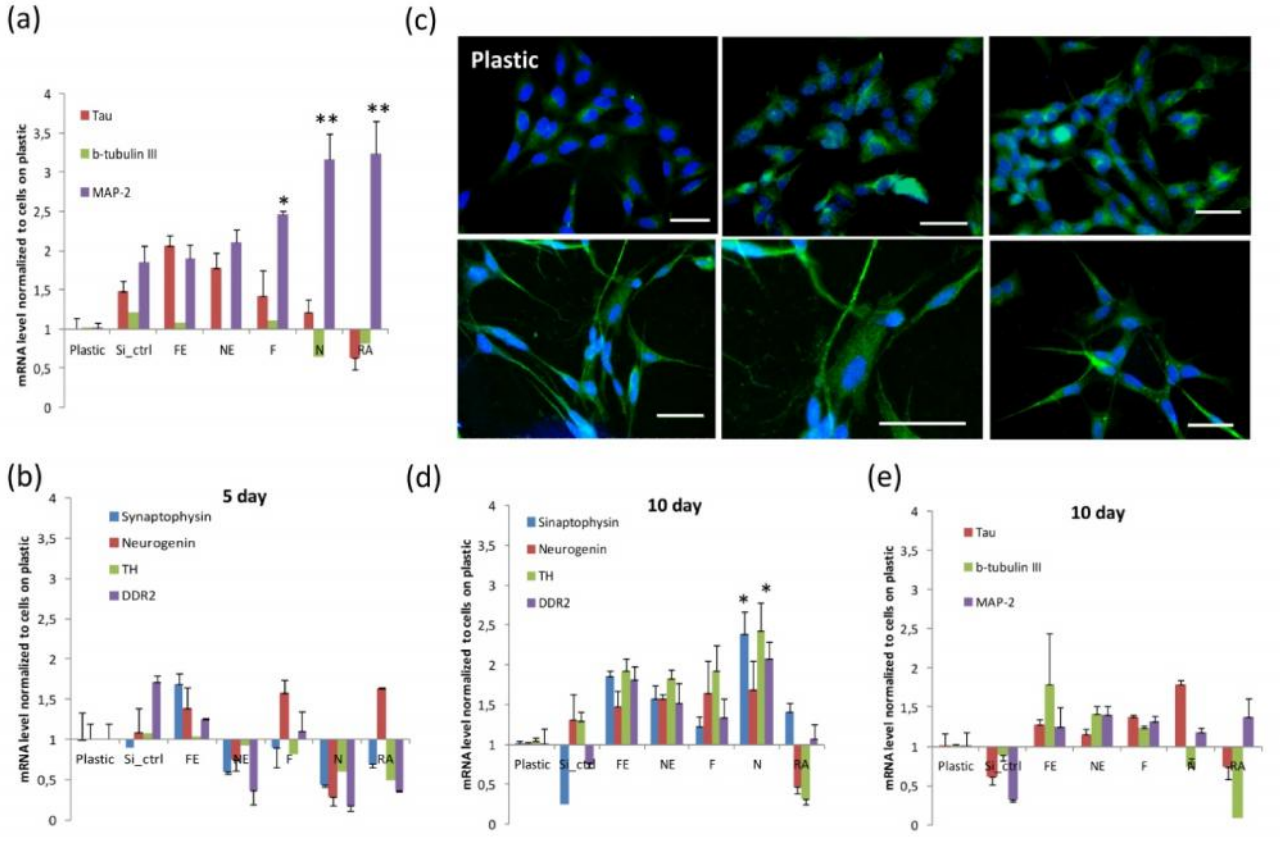
(a)
Tau
b-tubulin III
MAP-2
mRNA level normalized to cells on plastic
Plastic
Si_ctrl
FE
NE
F
N
RA
(c)
Plastic
(b)
5 day
Synaptophysin
Neurogenin
TH
DDR2
(d)
10 day
Sinaptophysin
(e)
10 day

Fig 5

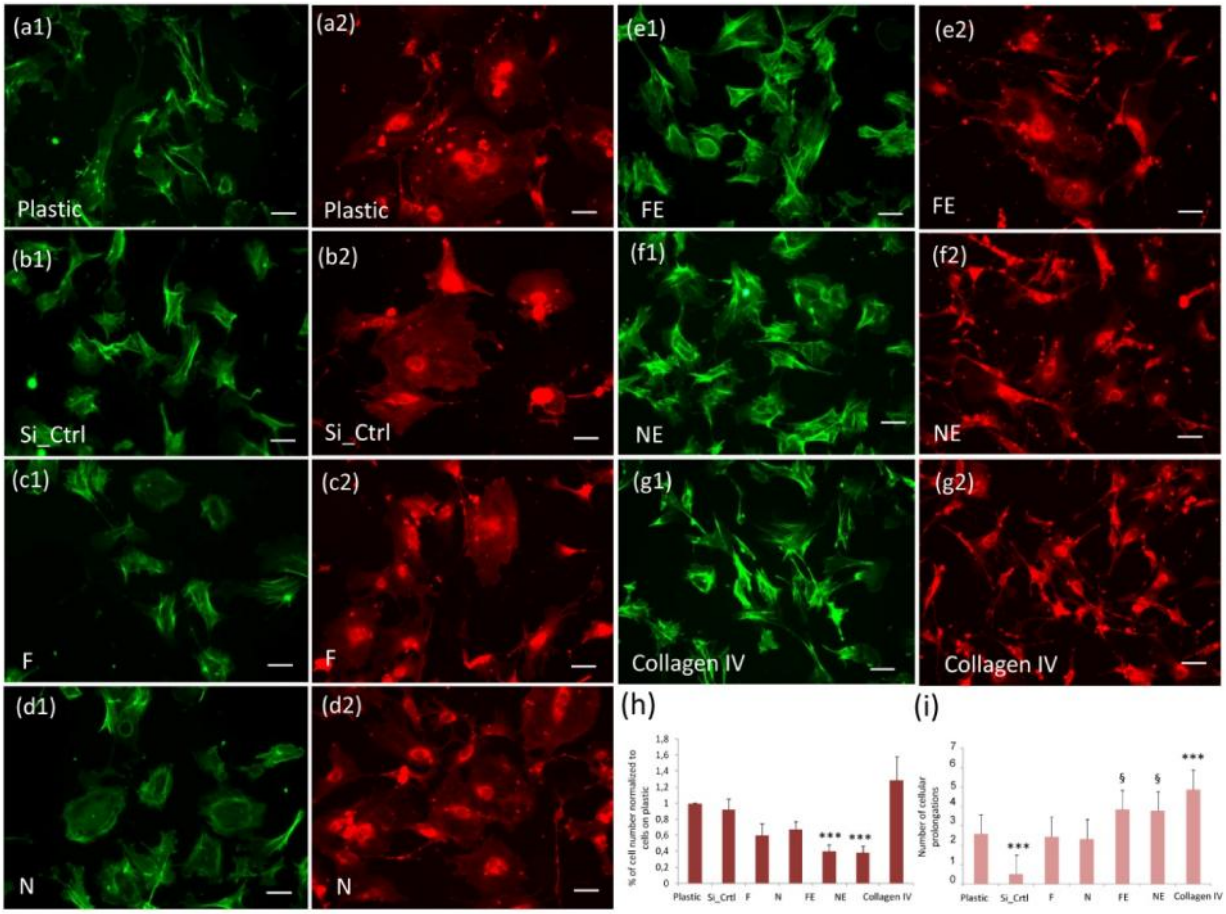
(a1)
Plastic
(a2)
Plastic
(e1)
FE
(e2)
FE
(b1)
Si_Ctrl
(b2)
Si_Ctrl
(f1)
NE
(f2)
NE
(c1)
F
(c2)
F
(g1)
Collagen IV
(g2)
Collagen IV
(d1)
N
(d2)
N
(h)
% of cell number normalized to cells on plastic
Plastic
Si_Crtl
F
N
FE
NE
Collagen IV
(i)
Number of cellular prolongations
Plastic
Si_Crtl
F
N
FE
NE
Collagen IV

Fig 6

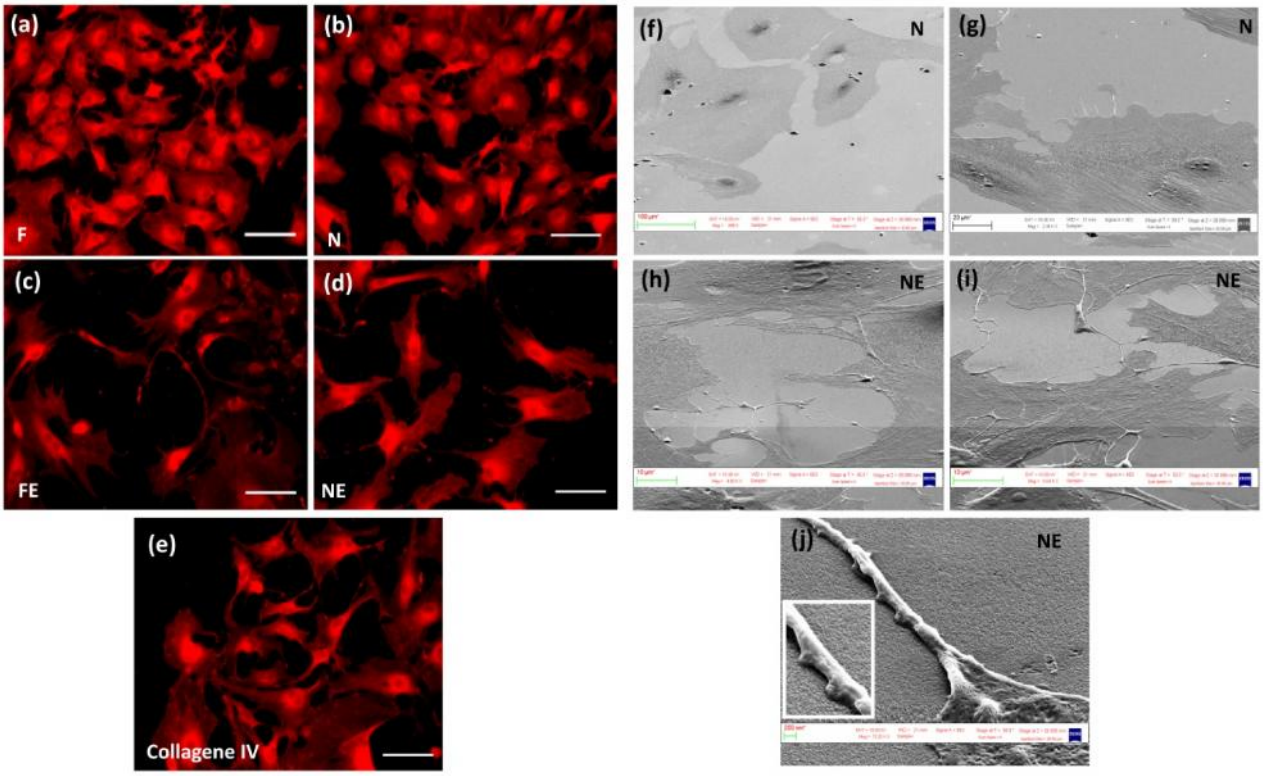

Fig 7

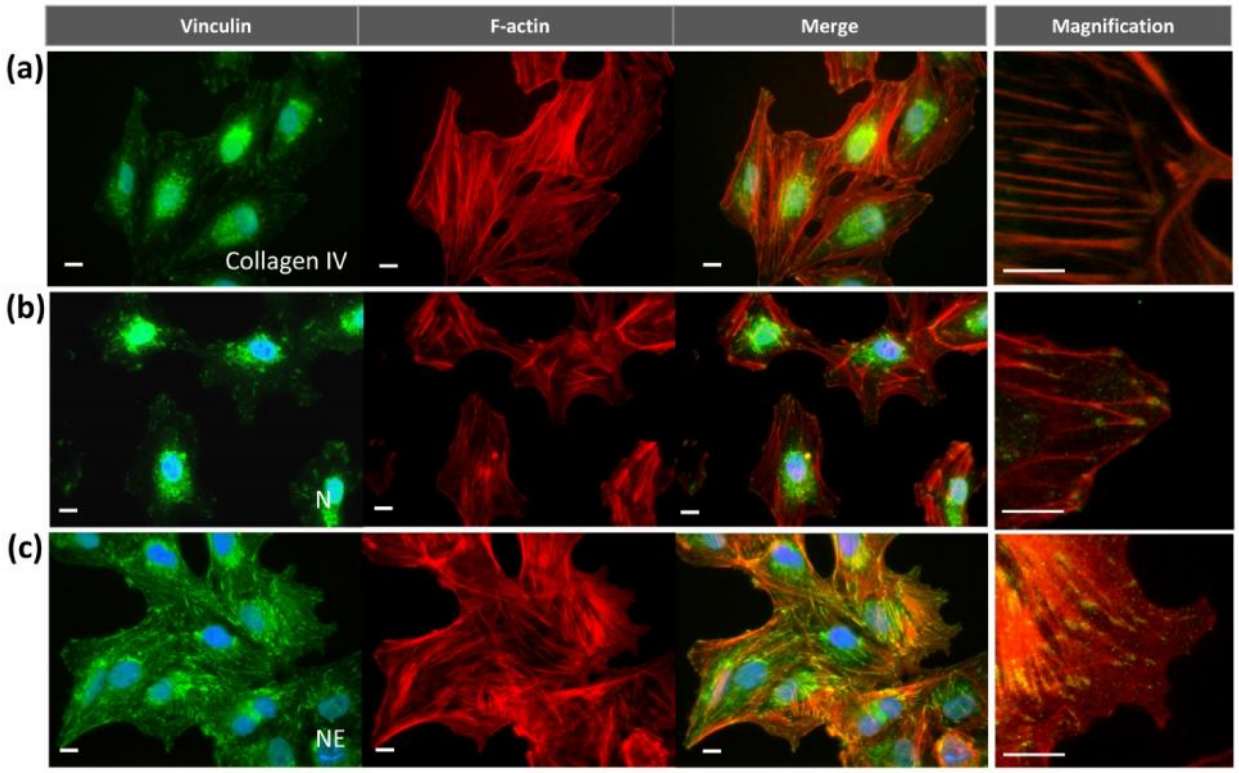

Fig 8

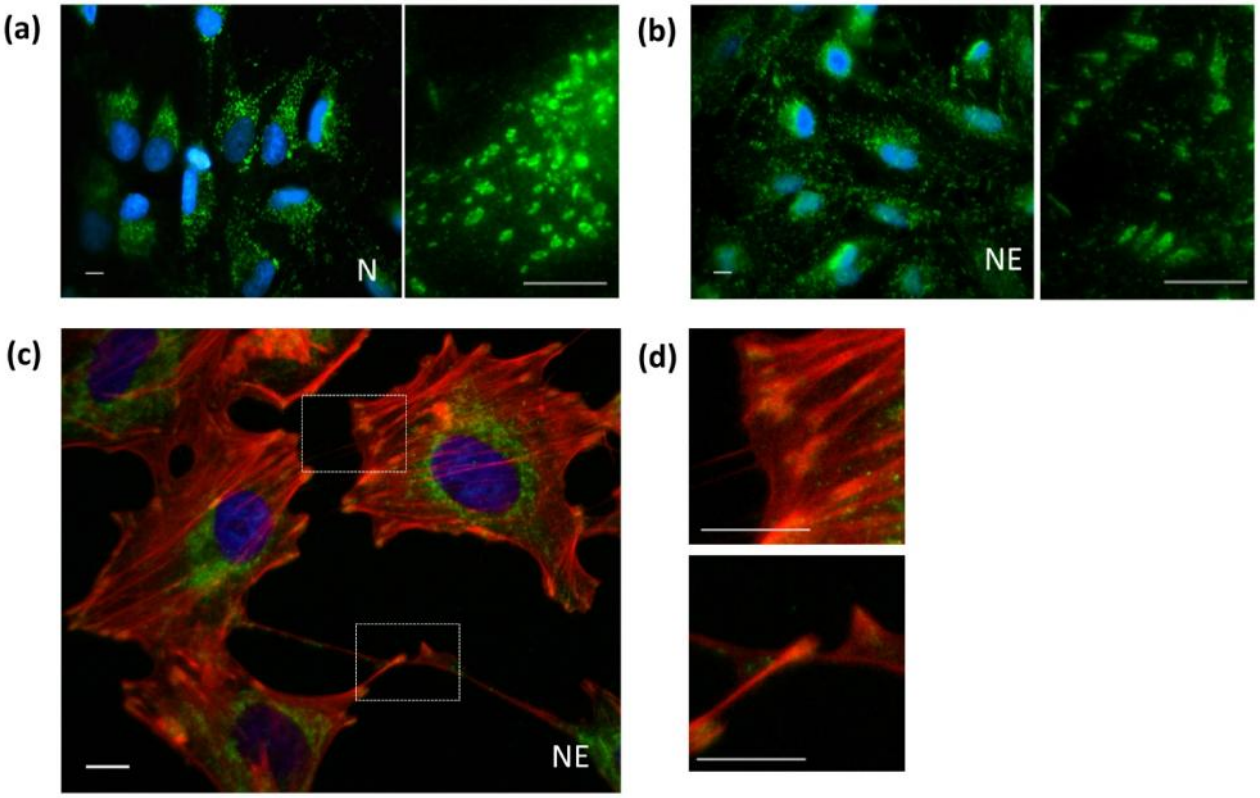

Fig 9

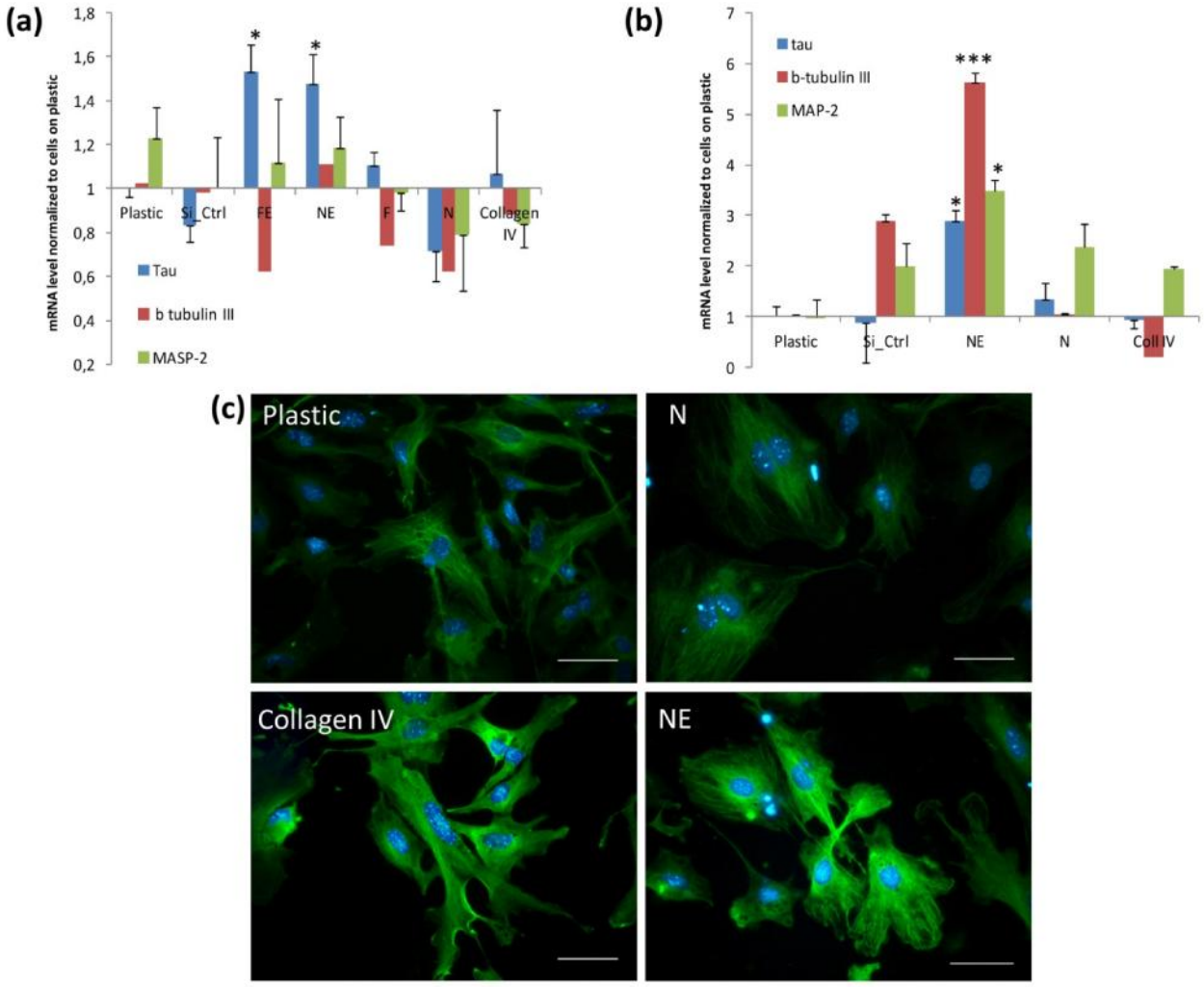
(a)
mRNA level normalized to cells on plastic
1,8
1,6
1,4
1,2
1
0,8
0,6
0,4
0,2
Plastic
Si_Ctrl
FE
NE
F
N
Collagen IV
Tau
b tubulin III
MASP-2
(b)
mRNA level normalized to cells on plastic
7
6
5
4
3
2
1
0
tau
b-tubulin III
MAP-2
Plastic
Si_Ctrl
NE
N
Coll IV
(c)
Plastic
N
Collagen IV
NE

Fig 10

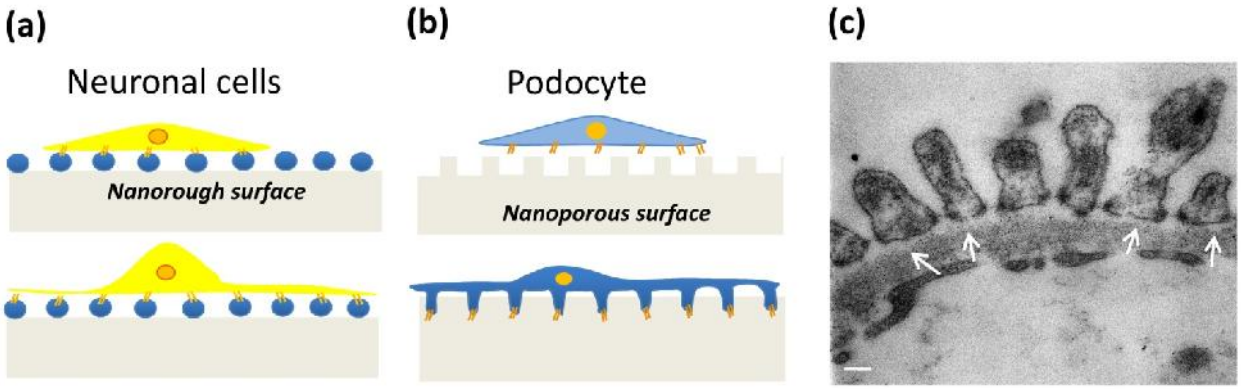
(a)
Neuronal cells
Nanorough surface
(b)
Podocyte
Nanoporous surface
(c)

Fig 11

Substrate	Average island/pillar size (nm^2)	Surface area coverage (%)	Amplitude	Organization	
			Surface roughness (rms)	Surface density (%)	Fractal dimension
F	163	54	0.88 nm	67.6	2.84
FE	405	35	0.80 nm	35.97	2.79
N	69	38	1.20 nm	33.67	2.79
NE	775	53	0,63 nm	63.71	2.89

Tab 1